Heat Balance in the Nocturnal Boundary Layer during CASES-99

JIELUN SUN,* SEAN P. BURNS, ANTHONY C. DELANY, STEVEN P. ONCLEY, THOMAS W. HORST,
AND DONALD H. LENSCHOW

National Center for Atmospheric Research,+ Boulder, Colorado

(Manuscript received 17 April 2002, in final form 1 May 2003)

ABSTRACT

A unique set of nocturnal longwave radiative and sensible heat flux divergences was obtained during the 1999 Cooperative Atmosphere–Surface Exchange Study (CASES-99). These divergences are based on upward and downward longwave radiation measurements at two levels and turbulent eddy correlation measurements at eight levels. In contrast to previous radiation divergence measurements obtained within 10 m above the ground, radiative flux divergence was measured within a deeper layer—between 2 and 48 m. Within the layer, the radiative flux divergence is, on average, comparable to or smaller than the sensible heat flux divergence. The horizontal and vertical temperature advection, derived as the residual in the heat balance using observed sensible heat and radiative fluxes, are found to be significant terms in the heat balance at night. The observations also indicate that the radiative flux divergence between 2 and 48 m was typically largest in the early evening. Its magnitude depends on how fast the ground cools and on how large the vertical temperature gradient is within the layer. A radiative flux difference of more than 10 W m^{-2} over 46 m of height was observed under weak-wind and clear-sky conditions after hot days. Wind speed variation can change not only the sensible heat transfer but also the surface longwave radiation because of variations of the area exposure of the warmer grass stems and soil surfaces versus the cooler grass blade tips, leading to fluctuations of the radiative flux divergence throughout the night.

1. Introduction

Numerous observational studies have demonstrated the application of Monin–Obukhov (M–O) similarity theory (Monin and Obukhov 1954) to unstable boundary layers. In contrast, stable boundary layers are less studied, and the validity of M–O similarity theory, which traditionally requires less than 10% turbulence divergence in the surface layer and negligible radiative flux divergence, is still uncertain under strongly stable conditions. The classic or ''textbook'' nocturnal boundary layer (NBL) is based mainly on weakly and moderately stable boundary layers in terms of observations (Van Ulden and Wieringa 1996; Mahrt et al. 1998), scaling arguments (Derbyshire 1990), similarity theory (Zilintinkevich and Mironov 1996), and laboratory studies (Ohya et al. 1997).

The importance of radiative cooling at night was recognized at least as far back as Glaisher (1847). Among the few observational studies of the radiative flux divergence in the literature, Funk (1960) first measured the radiative flux divergence at night and found that its contribution to clear-air cooling was always larger than the observed cooling in the lowest few meters. Similar results were also observed by Fuggle and Oke (1976), Roach et al. (1976), Nkemdirim (1978, 1988), Zhou and Chang (1982), and Moncrieff (1983) over different surface types. All of these studies measured the radiative flux at two levels below 10 m, where differences in the field of view (FOV) from the two pyrogeometers or two net radiometers were ignored or the surface was assumed to be homogeneous. None of these studies measured sensible heat flux. Under the assumption of no temperature advection in the heat balance, based on measured radiative flux divergence and local temperature trends, they concluded that the sensible heat flux must be convergent and must contribute to the local warming.

Based on sensible heat flux divergence observations, Kondo et al. (1978) and Howell and Sun (1999) found that, on average, the sensible heat flux was divergent in the lowest 10 m in the NBL and contributed significantly to cooling, instead of to warming as predicted by the previous studies mentioned above and by Elliott (1964). Sensible heat flux divergence can be complicated by

* Additional affiliation: Program in Atmospheric and Oceanic Sciences, University of Colorado, Boulder, Colorado.

+ The National Center for Atmospheric Research is sponsored by the National Science Foundation.

Corresponding author address: Jielun Sun, National Center for Atmospheric Research, 3450 Mitchell Lane, P.O. Box 3000, Boulder, CO 80307-3000.
E-mail: jsun@ucar.edu

differences in the intermittent turbulence at various heights associated with atmospheric disturbances such as density currents, solitary waves, and internal gravity waves (Sun et al. 2002, 2004).

The radiative flux divergence has also been studied using numerical models (Garratt and Brost 1981; André and Mahrt 1982; Li et al. 1983; Tjemkes and Nieuwstadt 1990; Räisänen 1996). Numerical results from Garratt and Brost (1981) and Li et al. (1983) suggest that the cooling in the lower part of the NBL, that is, the surface layer, is dominated by the radiative flux divergence, whereas the sensible heat flux divergence dominated the local cooling in the upper part of the NBL. Rider and Robinson (1951) and André and Mahrt (1982) concluded that both radiative and sensible heat flux contributed to the NBL cooling.

The largest radiative cooling is thought to occur during the evening transition period. During this period, water vapor is trapped close to the surface by the development of the stable boundary layer (Acevedo and Fitzjarrald 2001) and may form fog. The increased water vapor content enhances the radiative cooling of the fog layer up to 0.8°C h^{-1} below 50 m (Fitzjarrald and Lala 1989). As an additional complication, Funk (1960) and Zhou and Chang (1982) found that the vertical gradient of the radiative flux below 2 m oscillated during the night. This oscillation led to radiative flux convergence below 3 m, that is, clear-air warming, in the results of Funk (1960) and Nkemdirim (1978).

Whether radiative or sensible heat flux divergence dominates the local cooling, large vertical variations of either flux violate the condition of approximate height independence of turbulent fluxes within the surface layer, as required for M–O similarity theory, and contribute to the uncertainty of the stability functions under stable conditions. A constant turbulent flux layer may not even exist with the relatively large vertical divergence of the turbulent and radiative heat fluxes that can occur in stable boundary layers.

During the 1999 Cooperative Atmosphere–Surface Exchange Study (CASES-99; Poulos et al. 2002), vertical variations of radiative and sensible heat fluxes were carefully measured (section 2). In this study, we focus on the roles of radiative and sensible heat flux divergences in the heat balance at night, with discussions on comparisons between CASES-99 and previous observations (section 5). Detailed calculation of the longwave radiative flux divergence, adjusted for the different surface areas seen by the radiometers at two heights, is discussed in section 3. The heat balance is investigated in section 4, and the results are summarized in section 5.

2. Observations

CASES-99 was conducted about 5 km southeast of Leon, Kansas, during October of 1999 (Fig. 1). A 60-m tower at the main site was surrounded by six Integrated Surface Flux Facility (ISFF) 10-m towers (Sun et al. 2002). Surface types at each ISFF station are listed in Table 1. ISFF stations 1, 2, 3, and 5 included a radiation platform for longwave and net radiation measurements (Fig. 2). In addition, the incoming and outgoing shortwave radiation were measured at station 2. The radiation platform at each station was installed about 5–10 m away from the 10-m ISFF tower. The surface type at each 10-m ISFF tower and its radiation station were similar except at station 3, at which the platform viewed a mixture of senescent and tall green grass that was much thicker and taller than the grass surrounding the 10-m ISFF tower.

During the experiment, 10 Eppley Laboratory, Inc., precision infrared radiometers (model PIR) were deployed to measure the longwave radiative flux divergence. The 10 pyrgeometers were set on a long bench looking upward for intercomparison between 27 September and 5 October 1999 (Burns et al. 2000, 2003). After the in-field intercomparison period, four of the pyrgeometers were installed on a 5-m boom at 48 m on the 60-m main tower—two to measure the downward longwave radiative flux and two to measure the upward longwave radiative flux (Fig. 2). Among the remaining six pyrgeometers, two were installed at stations 1 and 2 to monitor the downward longwave radiation at 2-m height, and the other four pyrgeometers were installed at stations 1, 2, 3, and 5 to monitor the upward longwave radiation at 2-m height over the four dominant surface types surrounding the 60-m tower (Fig. 2). The sampling rate for all the radiometers was 0.2 s^{-1}.

The instruments used in this study also included sonic anemometers at eight levels (1.5, 5, 10, 20, 30, 40, 50, and 55 m), barometers (Paroscientific, Inc.) at three levels (1.5, 30, and 50 m), propeller-vane wind measurements at four levels (15, 25, 35, and 45 m), and aspirated Vaisala, Inc., 50Y Humitter sensors for temperature/humidity measurements at six levels (5, 15, 25, 35, 45, and 55 m). All of the above sensors, except the Humitter sensors, were mounted on 4-m booms, pointing to the east. The measurements from the sonic anemometers on the 60-m tower were sampled at 20 s^{-1}, and the remaining instruments were sampled at 1 s^{-1}. High-vertical-resolution air temperatures were also measured by thermocouples (E-type chromel–constantan, 0.0254-mm diameter) at 32 levels on the 60-m tower and 2 levels on two adjacent minitowers (Burns and Sun 2000). The sampling rate for the thermocouples was 5 s^{-1}.

Each ISFF tower included a sonic anemometer at 5 m, a propeller vane for wind measurements at 10 m, a barometer (Vaisala PTB220B) and a Vaisala temperature/humidity sensor at 2 m above the ground, and an Everest Interscience, Inc., narrowband infrared (IR) radiometer at 10 m at an angle of 45° from nadir. The sampling rate at the ISFF towers was 20 s^{-1} for the sonic anemometers, 1 s^{-1} for the IR radiometer and the propeller vane, and 0.2 s^{-1} for the remaining measurements.

In this study, central standard time (CST), which is

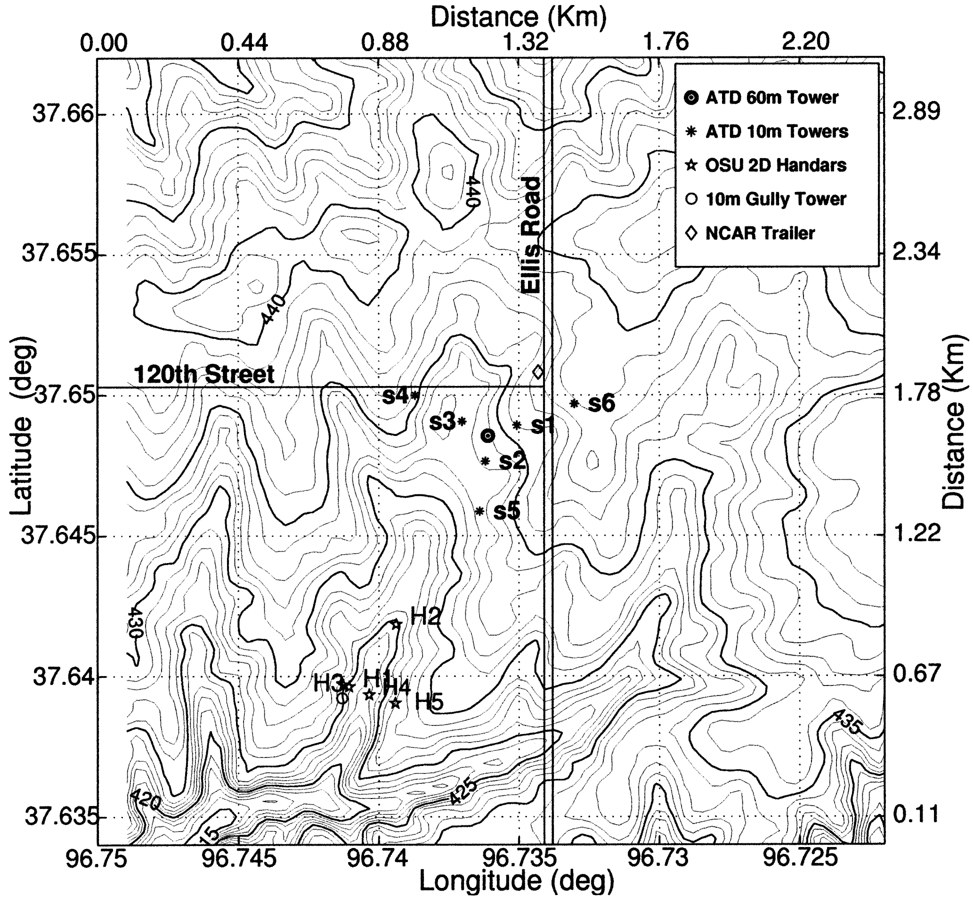

FIG. 1. The 60-m tower and the six ISFF 10-m towers (S1, . . . , S6). The contour lines of the surface topography are in meters.

6 h behind UTC, is used. Howell and Sun (1999) demonstrated that most of the turbulence can be captured with a time window of 10 min under stable conditions, which implies that turbulence intermittency does not significantly affect the turbulent flux statistics using the fixed window size. However, the timing of the turbulence intermittency at different heights does affect the vertical variation of turbulent flux with time, as demonstrated by Sun et al. (2002, 2004). In this study, we focus on one night and a monthly averaged study of the heat balance. For the case study, turbulent flux profiles are calculated using unweighted perturbations from data windows that vary with time so that mesoscale/large-eddy influences are excluded and turbulence intermittency is properly handled (Howell and Mahrt 1997). For the monthly averaged heat balance, the turbulent fluxes are calculated using 5-min windows. On average, the difference of the sensible heat flux divergence calculated with the 5-min and variable windows is less than 10%.

The longwave radiative flux is obtained from a pyrgeometer by using measurements of dome and case temperatures, and output from a thermopile (Burns et al. 2003). The coefficients for calculating the dome and case temperatures and thermopile output for each pyrgeometer were calibrated in the laboratory and were optimized from the in-field intercomparison period to increase their relative accuracy. On average, the in-field intercomparison reduces the relative difference between the pyrgeometers from ± 0.75 to less than ± 0.4 W m^{-2}. The measurement from the pyrgeometer deployed at station 1 for downward longwave radiation is much different than that from the rest of the pyrgeometers. Because there are no apparent physical reasons for any significant differences, we discard it from the study.

TABLE 1. Surface types at the four radiation stations (1, 2, 3, and 5) and two ISFF tower sites (4 and 6).

Station No.	Surface types
1	Mixture of short green and brown grass (~0.1 m)
2	Dominated by various short grasses mixed with bluestem grass (~0.5 m)
3	Mixture of senescent and green tall grass (~0.3 m)
4	Tall grass (>0.3 m)
5	Mixture of tall sparse green weeds (~0.3 m) with very fine short weed grass (~0.15 m)
6	Grass similar to station 1, but with rocky ground

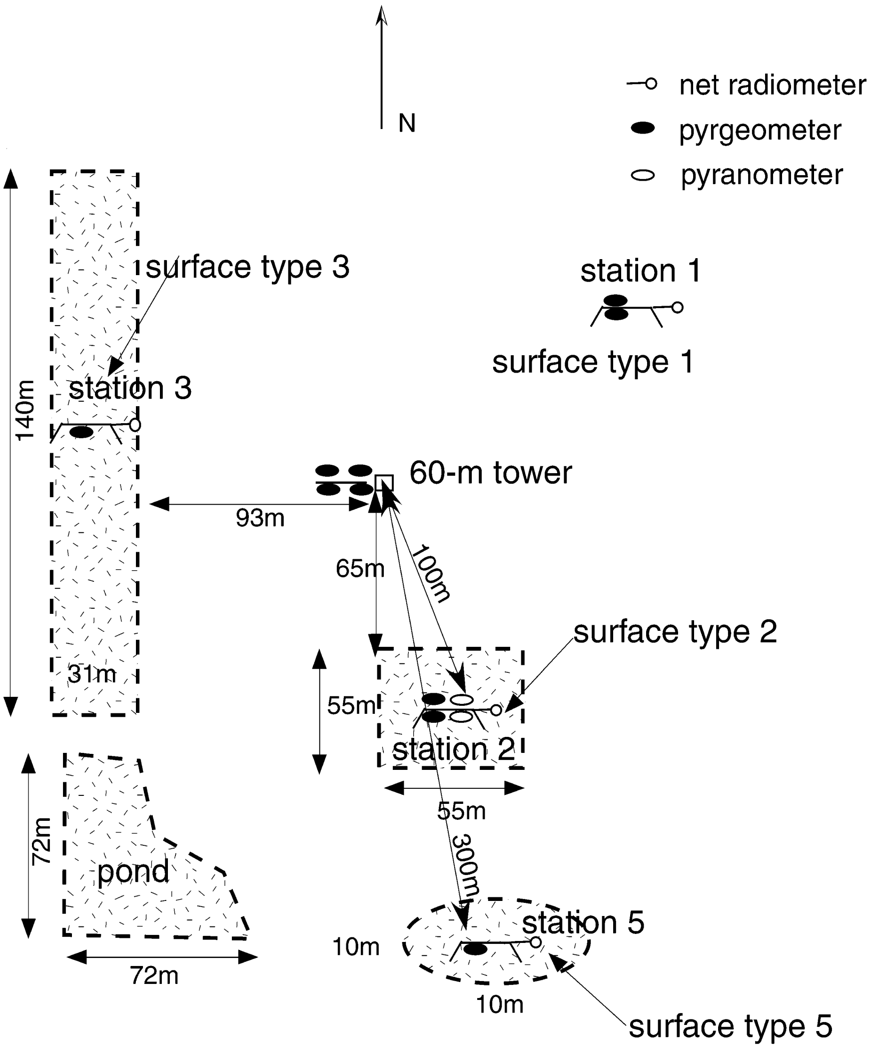

FIG. 2. Schematic diagram of the 10-pyrgeometer deployment, four net radiometers, and two pyranometers, and the land surface types (see Table 1) and coverage.

3. Calculating longwave radiative flux divergence over heterogeneous surfaces

The radiative flux divergence is traditionally measured by four pyrgeometers or two net radiometers on a tower, one directly above the other. By doing so, the downward-looking pyrgeometer at the upper level "sees" a larger surface area than the one at the lower level. The difference between the measured longwave radiation at the two levels can be obscured by the different FOV of the two pyrgeometers if the surface is heterogeneous. The FOV of the 2-m downward-looking pyrgeometer is small enough that it can be assumed to be homogeneous, as assumed in previous studies. This is not the case at 48 m. To estimate the ground area seen by the pyrgeometer at 48 m, we can examine the outgoing longwave radiation measured by the downward-looking pyrgeometer through radiation transfer theory without emission from the atmosphere. The ground contribution to the outgoing longwave radiation measured at 48 m can be formulated as the longwave radiation intensity I (i.e., radiation energy integrated over wavelengths) emitted from the ground impinging on the radiometer integrated over a hemisphere (Liou 1980),

$$I^{\uparrow}_{48\mathrm{m}}(\text{ground}) = \int_0^{2\pi}\int_0^{\pi/2} I\cos\theta\, d\Omega = \int_0^{2\pi}\int_0^{\pi/2} I\cos\theta\sin\theta\, d\theta\, d\psi = \frac{1}{2}\int_0^{\pi}\int_0^{\pi/2} I\sin(2\theta)\, d\theta\, d\psi. \quad (1)$$

Here, Ω is the solid angle, and θ and ψ are the nadir and the azimuthal angles, respectively. Assuming the ground surface is isotropic so that the radiation intensity

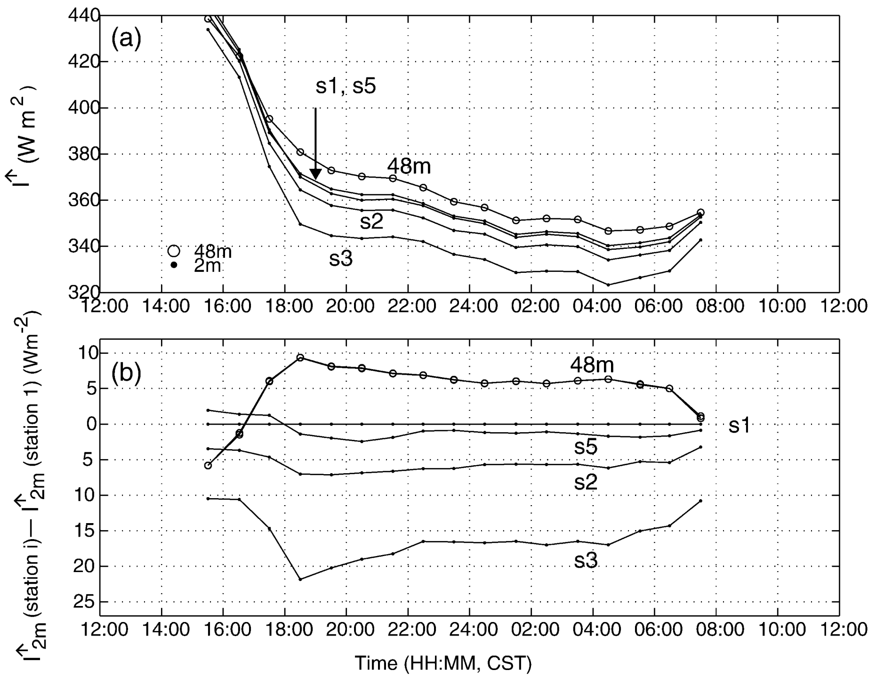

FIG. 3. (a) The upward longwave radiation at 2 m from the four radiation stations (S1, S2, S3, and S5) and at 48 m on the 60-m tower. (b) The differences between all the radiation measurements in (a) and the upward longwave radiation at station 1. Here all the diurnal variation from each pyrgeometer was averaged for the entire period of the field campaign.

from the ground is directionally independent, from (1) the measured upward longwave radiation $I^{\uparrow}$ over a uniform surface is

$$I^{\uparrow} = I\pi. \tag{2}$$

Because we had only a limited number of pyrgeometers, we simplified the area seen by the 48-m downward-looking pyrgeometer into five quasi-homogeneous surface types: four of them were land surfaces, which were monitored by four downward-looking pyrgeometers at 2 m, and the fifth was a pond (Fig. 2). Because the view angle of surface type 5 from the pyrgeometer at 48 m is larger than 81°, its contribution to the upward longwave radiation at 48 m is much smaller than the other four surface types and is neglected. Although the surface varied somewhat within each surface type, the variation among the surface types is much more significant (Fig. 3). During the field campaign, the pond temperature was measured several times with a handheld Everest IR radiometer, and was found to be $T_w = 288.15$ K. Assuming that the temporal and spatial variation of the pond surface temperature is relatively small in comparison with its absolute temperature, the longwave radiation emitted by the pond at night can be calculated as

$$I_w^{\uparrow} = \epsilon\sigma T_w^4. \tag{3}$$

Here, the emissivity $\epsilon = 0.96$ for water surface is used (Campbell and Norman 1998), and σ is the Stefan–Boltzmann constant.

Substituting (2) into (1), the ground contribution to the longwave radiation at 48 m can be simplified based on the schematic diagram of the surface survey in Fig. 2,

$$\begin{aligned} I_{48\mathrm{m}}^{\uparrow}(\text{ground}) &= \frac{1}{2\pi}\left[\int_0^{2\pi}\int_0^{\pi/2} I_1^{\uparrow}\sin(2\theta)\,d\theta\,d\psi \right. \\ &\quad + \int_0^{\psi_1}\int_{\theta_1}^{\theta_2} (I_2^{\uparrow} - I_1^{\uparrow})\sin(2\theta)\,d\theta\,d\psi \\ &\quad + \int_{3\pi/2-\psi_2}^{3\pi/2+\psi_2}\int_{\theta_4}^{\theta_5} (I_3^{\uparrow} - I_1^{\uparrow})\sin(2\theta)\,d\theta\,d\psi \\ &\quad \left. + \int_{3\pi/2+\psi_2}^{3\pi/2+\psi_2+\psi_3}\int_{\theta_8}^{\theta_7} (I_w^{\uparrow} - I_1^{\uparrow})\sin(2\theta)\,d\theta\,d\psi\right], \end{aligned} \tag{4}$$

where the angles are schematically illustrated in Fig. 4. In (4), $I_1^{\uparrow}$, $I_2^{\uparrow}$, and $I_3^{\uparrow}$ represent the longwave radiation measured from surface types at stations 1, 2, and 3, respectively. The influence of the tower structure is negligible because of its small FOV relative to the ground in the pyrgeometer hemispheric view as shown in appendix A.

Using the surface survey listed in Table 2 and (4), the integrated contribution of the ground emission to the pyrgeometer at 48 m is

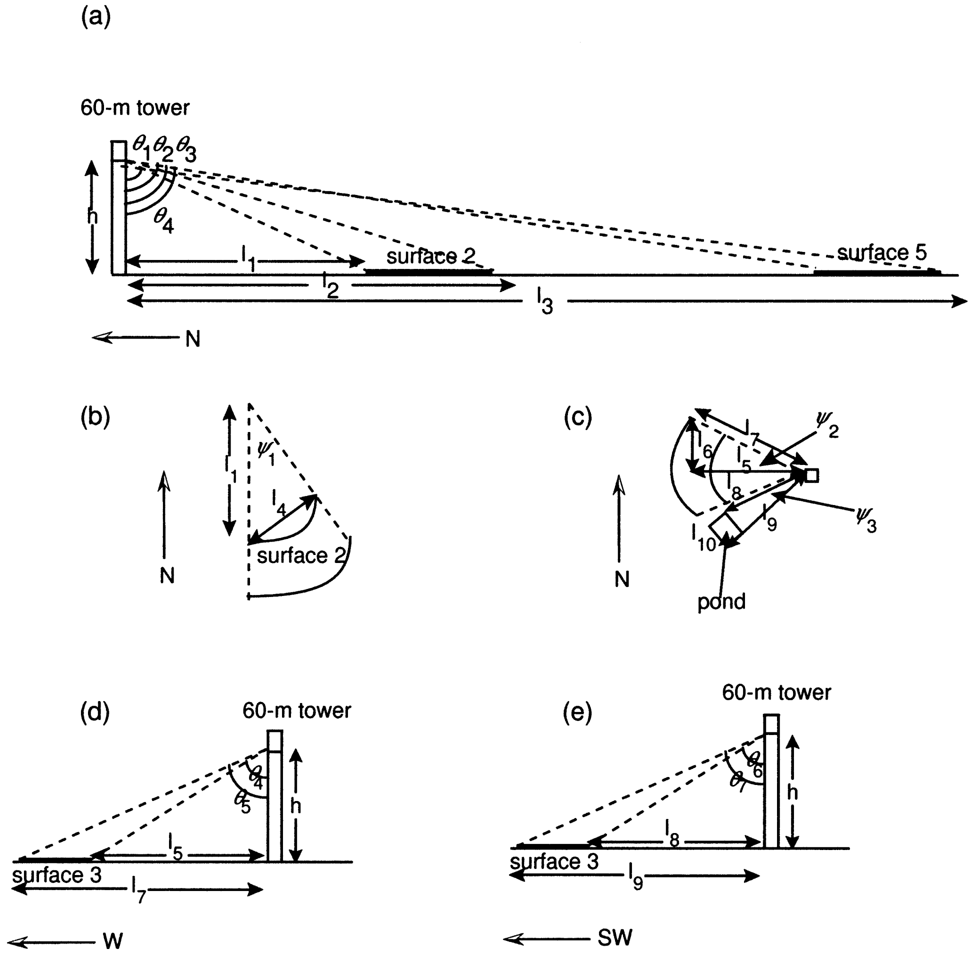

FIG. 4. Schematic diagram of all the input parameters related to the angles used in (4).

$$I^{\uparrow}_{48\mathrm{m}}(\mathrm{ground}) = 0.94I^{\uparrow}_1 + 0.03I^{\uparrow}_2 + 0.02I^{\uparrow}_3 + 0.01I^{\uparrow}_w. \tag{5}$$

Equation (5) indicates that the ground contribution from the surface types other than surface type 1 to the longwave radiation measured at 48 m is small. The frequency distribution of measured $I^{\uparrow}_{48\mathrm{m}}$ over the entire month is very similar to the distribution measured at 2 m at station 1, lending further support to the results in (5). The coefficients for $I^{\uparrow}_1$, $I^{\uparrow}_2$, $I^{\uparrow}_3$, and $I^{\uparrow}_w$ in (5) represent the integrated contribution of each surface type to the upward longwave radiation at 48 m, considering the size of each surface type and its location relative to the 48-m pyrgeometer.

To obtain the true radiative flux divergence, the area contribution of each surface type to the upward longwave radiation at both 2 and 48 m should be the same. Therefore, the same surface-type contributions to the longwave radiation as in (5) are used for estimating the integrated upward longwave radiation at 2 m for the same FOV as at 48 m, which is relevant for calculating the upward radiative flux divergence. Using the measured downward longwave radiation at 48 m ($I^{\downarrow}_{48\mathrm{m}}$) and at 2 m at station 2($I^{\downarrow}_{2\mathrm{m}}$), the measured upward longwave radiation at 48 m ($I^{\uparrow}_{48\mathrm{m}}$),and the calculated integrated radiation at 2 m adjusted for the 48-m FOV ($I^{\uparrow}_{2\mathrm{m}}$), the vertical longwave radiation divergence between 2 and 48 m can be estimated as

$$\Delta I|^{48\mathrm{m}}_{2\mathrm{m}} = \Delta I_{48\mathrm{m}} - \Delta I_{2\mathrm{m}} = I^{\downarrow}_{48\mathrm{m}} - I^{\downarrow}_{2\mathrm{m}} - I^{\uparrow}_{48\mathrm{m}} + I^{\uparrow}_{2\mathrm{m}}, \tag{6}$$

where $\Delta I = I^{\downarrow} - I^{\uparrow}$ is the net longwave radiative flux at any level. Measurement errors in $\Delta I|^{48\mathrm{m}}_{2\mathrm{m}}$ can be estimated as

$$\delta\Delta I|^{48\mathrm{m}}_{2\mathrm{m}} = [(\delta I^{\downarrow}_{48\mathrm{m}})^2 + (\delta I^{\downarrow}_{2\mathrm{m}})^2 + (\delta I^{\uparrow}_{48\mathrm{m}})^2 + (\delta I^{\uparrow}_{2\mathrm{m}})^2]^{1/2}. \tag{7}$$

Using the standard deviations of each pyrgeometer calculated during the in-field intercomparison period (Burns et al. 2003), the measurement error of $\Delta I|^{48\mathrm{m}}_{2\mathrm{m}}$ is estimated as 0.6 W m^{-2}.

4. Nocturnal heat balance

The heat balance within the layer between 2 and 48 m can be expressed as (e.g., Stull 1988)

TABLE 2. Input parameters in Figs. 4 and A1.

Parameter	l_1	l_2	l_3	l_4	l_5	l_6	l_7	l_8	l_9	l_{10}	h	H	l	w
(m)	65	120	300	55	93	70	124	120	189	100	48	60	5	1.3
Angles	θ_1	θ_2	θ_3	θ_4	θ_5	θ_6	θ_7	ψ_1	ψ_2	ψ_3	α	β_1	β_2	
(°)	52	67	81	62	68	67	75	40	37	45	7.4	84.3	63.4	

$$\int_{2\mathrm{m}}^{48\mathrm{m}} \left[\frac{\partial\overline{\theta}}{\partial t} + \frac{\partial(\overline{u}\,\overline{\theta})}{\partial x} + \frac{\partial\overline{u'\theta'}}{\partial x} + \frac{\partial\overline{w'\theta'}}{\partial z} + \frac{\partial(\overline{w}\,\overline{\theta})}{\partial z}\right] dz$$

$$= \int_{2\mathrm{m}}^{48\mathrm{m}} \left(\frac{\overline{T}}{\overline{\theta}c_p}\frac{\partial\Delta I}{\partial z}\right) dz \simeq \frac{\Delta I|_{2\mathrm{m}}^{48\mathrm{m}}}{c_p}, \qquad (8)$$

where $\overline{\theta}$ and $\overline{T}$ are the mean potential temperature and temperature, $\overline{\theta} \simeq \overline{T}$, c_p is the specific heat at constant pressure, $\overline{u}$ and $\overline{w}$ are the mean horizontal and vertical wind speeds, $\overline{w'\theta'}$ and $\overline{u'\theta'}$ are the vertical and horizontal turbulent sensible heat fluxes, and x and z are the along-wind and vertical coordinates, respectively. There was no liquid water in the layer; therefore, the variation of the latent heat flux only affects the water vapor mass balance in the layer and does not contribute to the heat balance in this layer. Equation (8) indicates that the local cooling ($\partial\overline{\theta}/\partial t$) is controlled by the horizontal and vertical temperature advection [$\partial(\overline{u}\,\overline{\theta})/\partial x$ and $\partial(\overline{w}\,\overline{\theta})/\partial z$], the sensible heat flux divergence ($\partial\overline{w'\theta'}/\partial z$) and ($\partial\overline{u'\theta'}/\partial x$), and the radiative flux divergence ($\partial\Delta I/\partial z$, i.e., radiative cooling). To understand the detailed behavior of the nocturnal heat balance, we focus on one night on which the radiative flux divergence was relatively strong in the early evening.

a. The night of 21 October

On the night of 21 October in CST (22 October in UTC), the outgoing longwave radiation started to decrease sharply around 1700 CST as a result of radiative cooling at the ground (Fig. 5). At the same time, the air temperature decreased significantly at all the observation levels, especially close to the ground (Fig. 6). Between 1600 and 1900 CST, the radiative flux difference increased to about 13 W m^{-2} (i.e., about 0.97°C h^{-1}; Fig. 5a). Because the ground cooled through longwave radiative emission, the sensible heat flux became negative close to the ground while the residual heat flux above was still slightly positive or zero (Fig. 7). This condition was also found by Grant (1997). Between 1600 and 1900 CST, the vertical divergence of the sensible heat flux between 1.5 and 50 m was about 5 W m^{-2} (i.e., about

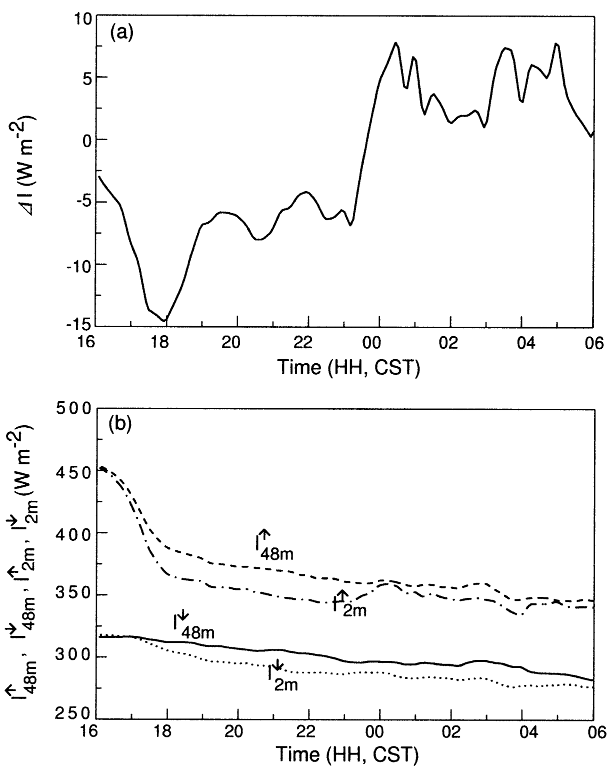

FIG. 5. (a) Net radiative flux difference between 2 and 48 m and (b) the measured incoming and outgoing longwave radiation components at 2 and 48 m for the night of 21 Oct.

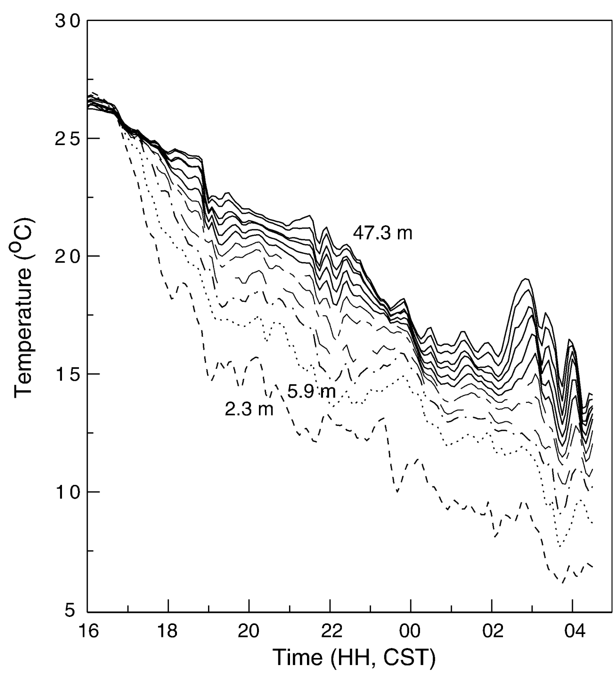

FIG. 6. Time series of the thermocouple temperature between 2 and 48 m for the night of 21 Oct. The height increment between adjacent levels is 1.8 m.

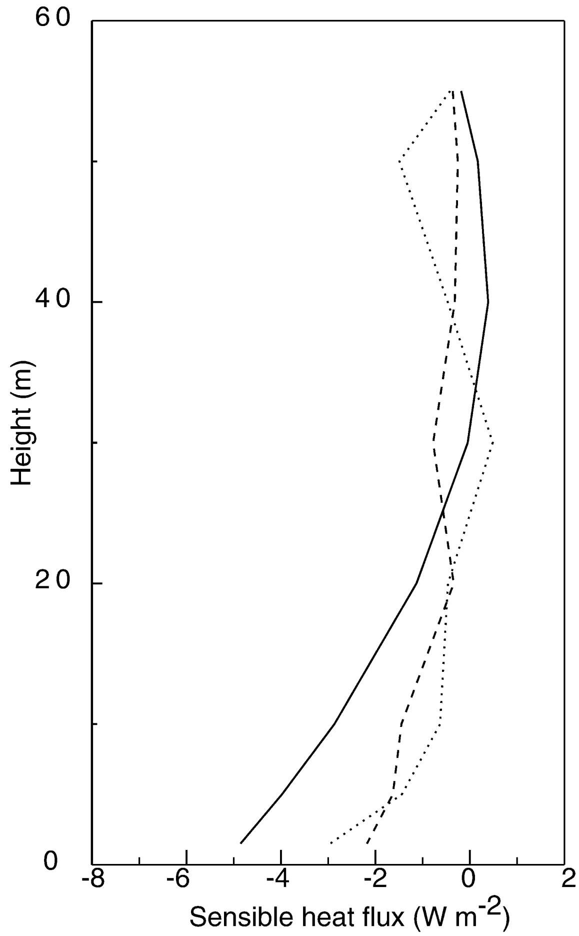

FIG. 7. Vertical profile of the sensible heat flux for 1600–1700 (solid line), 1700–1800 (dashed line), and 1800–1900 (dotted line) CST for the night of 21 Oct. The variable-window method is used for calculating the sensible heat flux.

0.4°C h^{-1}). The temperature decrease averaged between 2 and 48 m was about 2°C h^{-1} during the same period. The sum of the radiative and sensible heat flux divergences is about 1.4°C h^{-1}, which accounts for most of the local cooling. However, this also implies that the temperature advection and the horizontal turbulent heat transport also contribute significantly to the local cooling.

The spatial variation of the temperature at 2 m above the ground was found to vary with the surface elevation (Fig. 8). This height-dependent temperature distribution could be associated with the accumulated cold air transported by drainage flow in the area (Kobayashi et al. 1994), despite the observed ''uphill'' wind in Fig. 8. The largest elevation difference among the six ISFF stations is about 6 m, which leads to a negligible potential temperature correction of about 0.06°C to the spatial variation of the temperature at a constant height among the six stations. Based on the spatial variation of the temperature (about the same as the potential temperature) at 2 m from the six surface stations and the linearly extrapolated wind from 5 to 2 m, which was about 0.66 m s^{-1}, the estimated horizontal temperature advection at 2 m is about 4°C h^{-1}. Because of lack of information on the spatial variation of both wind and temperature between 2 and 48 m, the horizontal advection of temperature between 2 and 48 m and the horizontal turbulence flux divergence are unknown. If one assumes that the heat residual from the heat balance is entirely due to the horizontal temperature advection and uses the approximate wind speed of 3 m s^{-1} within the layer at the time, the horizontal temperature gradient needs to be about 0.05°C km^{-1} to obtain the heat residual of 0.6°C h^{-1}. This small horizontal temperature gradient is not measurable with towers separated by 100 m or even by 1 km in view of the absolute accuracy of current temperature measurements. If one assumes that the heat residual is entirely due to the vertical temperature advection and that the mean vertical velocity is negligible at 2 m when compared with that at 48 m, the mean vertical velocity at 48 m has to be about 3×10^{-5} m s^{-1} to contribute 0.6°C h^{-1} to the local cooling. Because of the complication of the tilt correction for sonic anemometers (Kaimal and Finnigan 1994), this accuracy for the mean vertical velocity was not possible in this experiment. The above advection analysis indicates that even a small horizontal or vertical temperature difference would contribute significantly to the local cooling.

b. Relationship between the temperature at 2 m and surface elevation

The elevation-dependent 2-m air temperature is clearly demonstrated in the air temperature difference between the lowest station (station 3) and the other stations (Fig. 9). The dependence of the air temperature on the surface elevation occurred only at night and was inversely related to the wind speed. When the wind speed is stronger than 5 m s^{-1}, strong turbulent mixing and advection eliminate temperature differences at various elevations and lead to a homogeneous temperature field. Similar results were also found by Harrison (1971), Geiger et al. (1995), LeMone and Grossman (2000), and Acevedo and Fitzjarrald (2001). This implies that to capture spatial variations of synoptic or ambient temperature, the temperature measurement height needs to be above the influence of surface drainage flows.

c. Relationship between the outgoing longwave radiation and wind

Around midnight CST of 21 October, the outgoing longwave radiation at 2 m increased by about 2–3 W m^{-2}; the incoming longwave radiation decreased steadily throughout the night (Fig. 5b). As a result, the radiative flux became convergent and fluctuated around zero thereafter (Fig. 5a). The time series of the surface radiation temperature T_r and the wind speed at the six ISFF stations (Fig. 10) indicate the dependence of the outgoing longwave radiation on the wind speed, although T_r observed

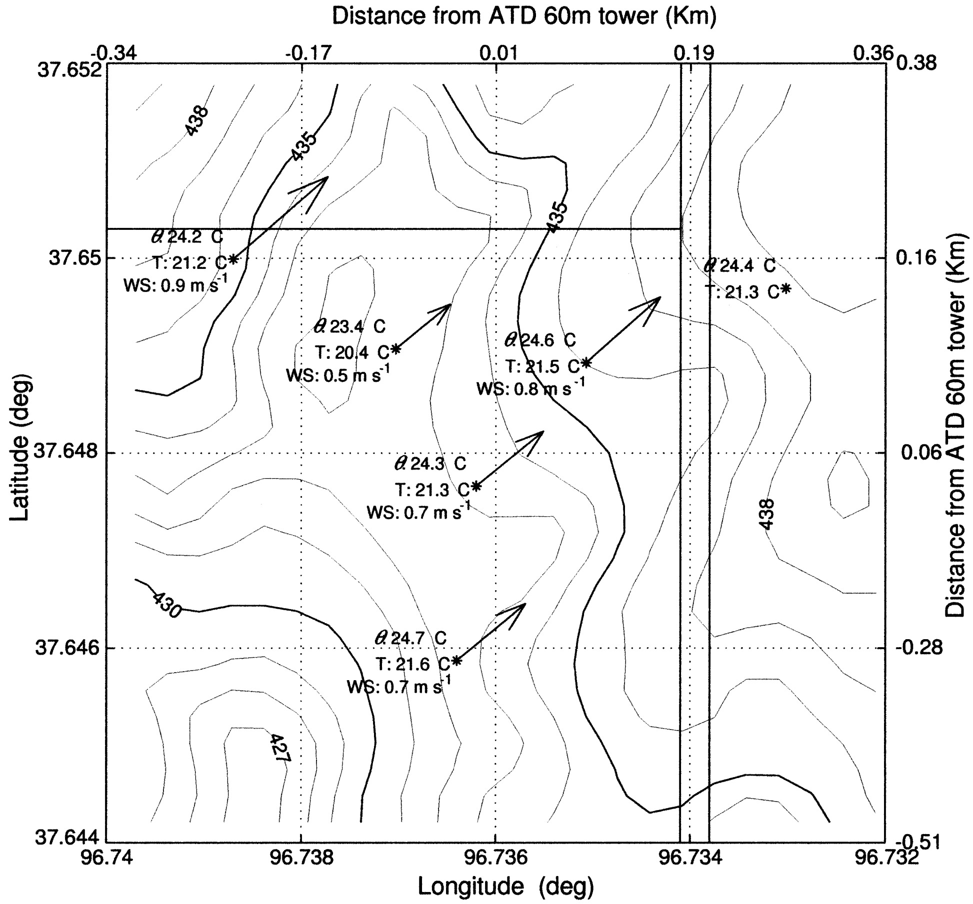

FIG. 8. Temperature, and wind speed and direction at 2 m between 1700–1800 CST at the six stations. The contour lines are the surface elevation in meters.

by the Everest radiometers was not as carefully monitored for accuracy as the pyrgeometers were.

Our field survey during CASES-99 showed that the variation of T_r was strongly influenced by vegetation at night. In general, the tips of the grass blades were colder than the dense stems of the grass and the top soil, which were protected by the grass blades from direct longwave cooling. As the wind speed increased, the warmer grass stems and soil surface were exposed through the bent grass. Therefore, the outgoing radiation temperature increased with wind speed. However, if relatively strong wind persists, the surface radiation temperature levels off after the initial increase due to heat loss through longwave emission, and eventually the radiative cooling of the soil surface and the grass stems reduces the outgoing longwave radiation. As the wind decreases, the cool grass blades reduce the outgoing longwave radiation. The larger variation of T_r at station 4 is due to its thicker and taller grass (Fig. 10). The relationship between the outgoing longwave radiation and wind speed at station 4 for the entire field campaign shows that, when wind speed is less than 5 m s^{-1}, the surface radiation temperature is related to the wind, but the relationship is not necessarily linear (Fig. 11). During daytime, the solar heating of the ground also contributes to T_r; therefore, there is no unique relationship between outgoing longwave radiation and wind speed. A similar vertical variation of the temperature within a grass layer was observed by Oke (1970), Sun (1999), and Qualls and Yates (2001).

Sun (1999) also reported that the heat source for the sensible heat flux over a grass layer was mainly from the middle level of the grass layer. Vining and Blad (1992) studied correlations between zenith angles of an infrared thermometer and sensible heat flux under constant solar angles. They found that the sensible heat flux was better correlated with the surface canopy temperature observed at the nadir and 20° from zenith when wind speed was stronger than 5 m s^{-1}. When the average wind speed was less than 4 m s^{-1}, 40° and 60° from zenith provided the best estimates of the sensible heat flux. Vining and Blad's results also implied that the surface radiation temperature varied with wind speed. In theory, sensitivity of the outgoing longwave radiation to wind speed variations depends on surface vegetation type and density, thermal inertia of the ground surface,

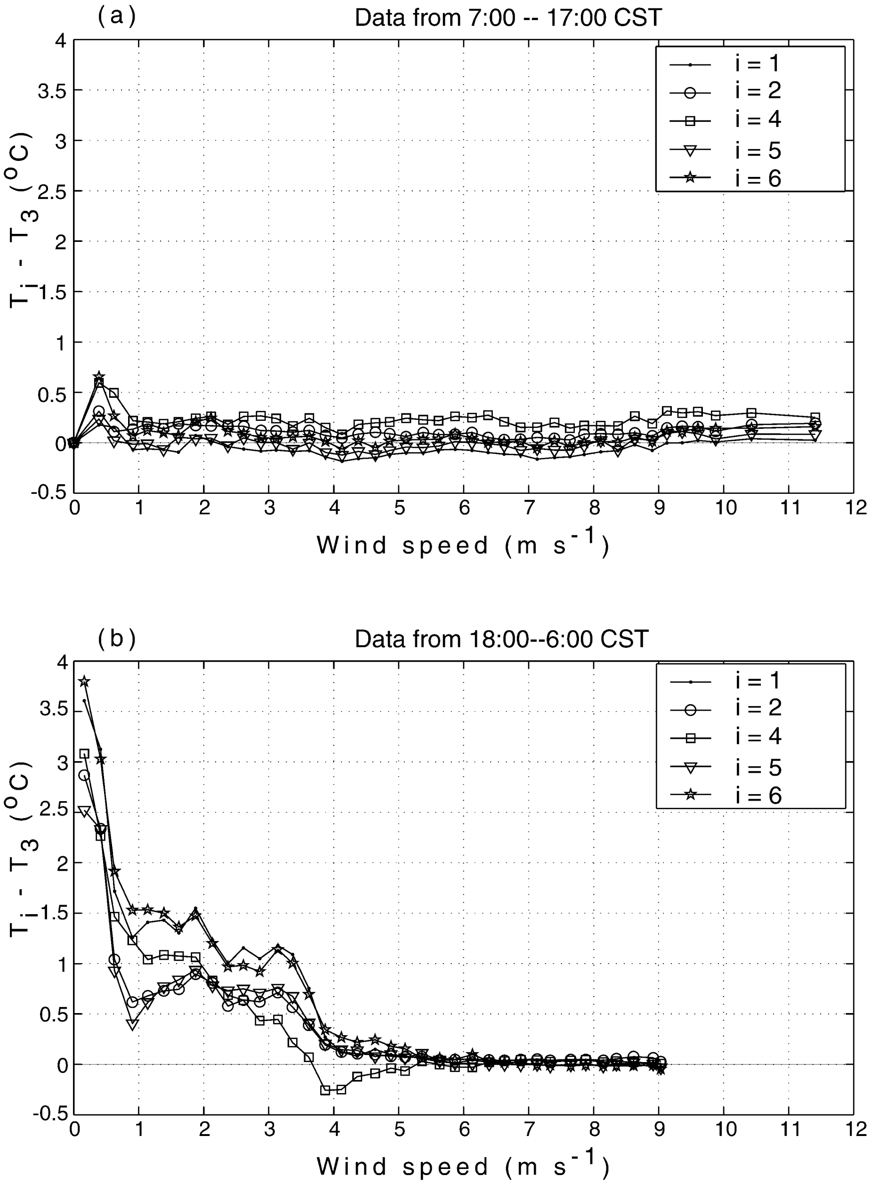

FIG. 9. Relationship between wind speed from the sonic anemometer at 5 m on the 60-m tower and the 2-m air temperature difference between station 3 and the rest of the five stations (a) during the daytime and (b) at night. The subscript *i* represents the station numbers. All of the curves are based on the 5-min-averaged data.

and how frequently the soil surface has been exposed. However, detailed study on this subject is beyond this experiment.

As the wind speed increased, downward transport of sensible heat flux also increased, leading to the air temperature increase. However, the observed air temperature increase within the layer when the radiative flux converged around midnight was, on average, less than the surface radiation temperature increase (Figs. 6 and 10) and did not follow the wind speed change as closely as did the surface radiation temperature. Our calculation in appendix B indicates that the surface radiation contributes about 80% of the outgoing longwave radiation measured at 2 m. Therefore, the variation of the surface radiation temperature and not the variation of the air temperature dominated the variation of the upward longwave radiation at 2 m.

d. Discussions of the current and previous heat balance studies

The previous studies mentioned in the introduction showed that the observed maximum net radiative flux difference between two levels under 10 m and clear-sky

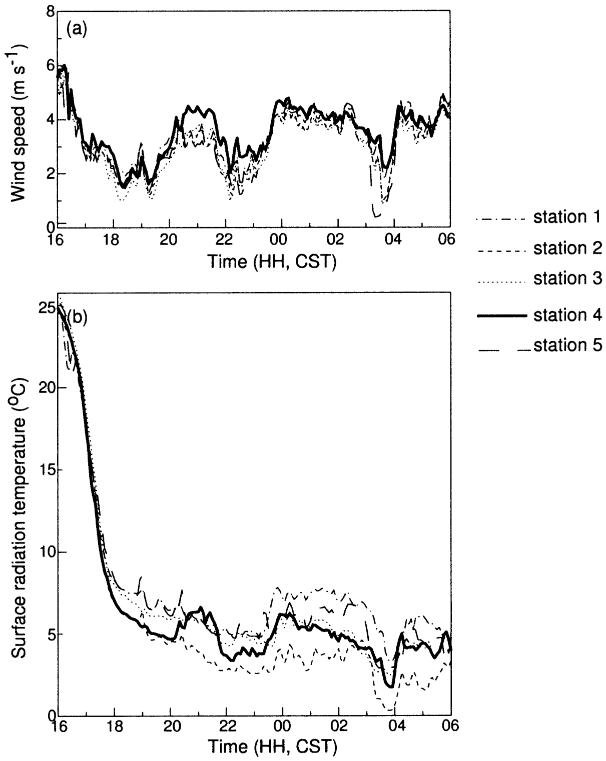

FIG. 10. Time series of (a) the wind speed and (b) the surface radiation temperatures at the six stations for the night of 21 Oct.

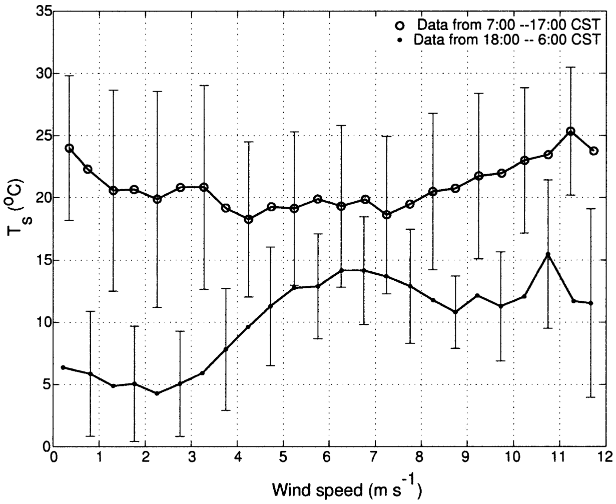

FIG. 11. Relationship between surface radiation temperature and the 10-m wind speed at station 4 during the daytime (circles) and at night (dots) for the entire field campaign. The curves are bin averaged based on the 5-min-averaged data. The standard deviation of the 5-min data within each bin is plotted in the figure.

conditions is less than 5 W m^{-2}. Our observed maximum net radiative flux difference between 2 and 48 m is larger than 10 W m^{-2}. The increase of the net radiative flux difference with the depth of the layer is consistent with radiation transfer theory. However, the previous studies found that the radiative cooling was typically stronger than the local cooling below 10 m, whereas our study indicates that the radiative flux divergence was weaker than the local cooling between 2 and 48 m, even during the largest radiative cooling night. Because the radiative cooling is the net radiative flux divergence, that is, the vertical gradient of the net radiative flux, the apparent contradiction between the previous studies and this study implies that the radiative flux divergence decreases with height. Decrease of the radiative flux divergence with height was also found by André and Mahrt (1982) and Li et al. (1983) through numerical simulations based on observed temperature and humidity profiles. Furthermore, a linear decrease of the radiative flux divergence has been commonly assumed in previous NBL studies (Yamada 1979; Nieuwstadt 1980; Lenschow et al. 1987).

Both local and radiative cooling decrease with height, and, in general, the absolute values of the sensible heat flux divergence decrease with height. However, the relative contributions of the sensible heat flux divergence, the radiative cooling, and the temperature advection (both horizontal and vertical) to the local cooling may vary with height. A increasing role of horizontal temperature advection to the local cooling with height was obtained through numerical models by Maki et al. (1986), and an increasing cooling with height by the sensible heat flux divergence was found by Elliott (1964), Garratt and Brost (1981), and Li et al. (1983).

The diurnal variation of the radiative flux divergence averaged over the entire field campaign shows that, on average, the radiative flux divergence is close to zero except in the early evening (Fig. 12). On average, the sensible heat flux divergence is about 30% of the local cooling. The relatively small averaged radiative flux divergence is partly due to the fluctuation of the ground longwave radiation emission with wind speed, as demonstrated earlier. The fluctuation of the surface radiation temperature is not captured in all of the numerical studies on the heat balance. Smith and Shi (1992) demonstrated the importance of the air–surface temperature difference at the ground in modeling the radiative cooling.

The relatively small contribution of both sensible heat flux divergence and the radiative cooling to the air cooling in this relatively deep layer implies that cold-air advection was important during CASES-99. Statistical analysis of the wind field during CASES-99 indicates that the wind was commonly from the south, in which direction the ground was lower than the 60-m tower, and the air that was advected into the tower area was colder. Similar diurnal variation of the total air cooling and the radiative cooling (both are large in the early evening) implies that longwave emission is the driving heat sink for cooling the NBL, although the magnitude of the air cooling at any location may be dominated by either the sensible heat transfer or the temperature advection. The sensible heat flux divergence and the tem-

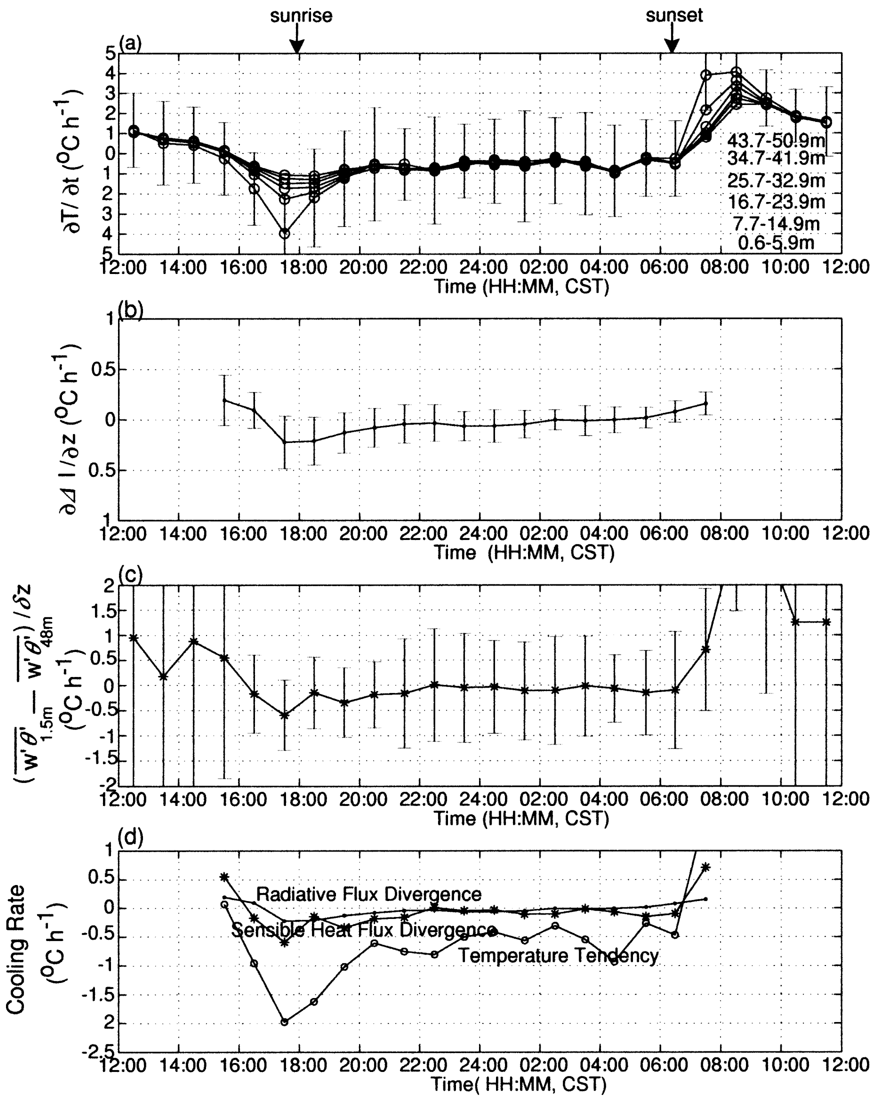

FIG. 12. (a) Thermocouple temperature tendency (different from the potential temperature by less than 1%) within various layers between 2 and 48 m (listed in the figure); (b) radiative flux divergence (negative); (c) sensible heat flux divergence between 2 and 48 m composited over the entire field experiment, and the standard deviations of each variable at each hour. Here both the temperature tendency and the sensible heat flux divergence are calculated using 5-min-averaged data. (d) The cooling rates of all measured components between 2 and 48 m.

perature advection are mechanisms for transferring heat that is ultimately lost to space by longwave radiation emission at night.

Averaged observations of the radiative flux divergence in both this study and that of Nunez and Oke (1976) demonstrated the diurnal variation of the radiative cooling, with the strongest cooling in the early evening, even though the observations in this study were over a relatively deep layer and Nunez and Oke's observations were below 5 m and within a canyon. This diurnal variation of the radiative flux divergence is related to the diurnal variation of wind speed. Rapid cooling in the early evening was also observed by Gustavsson et al. (1998).

e. Relevant factors on heat transfer terms and M–O similarity theory

The net radiative flux difference between 2 and 48 m in the early evening (between 1700 and 1800 CST) was largest for 21 and 25 October (Fig. 13). The maximum daytime surface radiation was highest on 21 October, following a 5-day warming trend, and was the second highest on 25 October, following a 3-day warming trend. In addition, the wind speed for those two nights was relatively low. The relationship among high maximum daytime radiation temperature, low wind, and large radiative flux divergence in the early evening indicates that the high maximum daytime radiation tem-

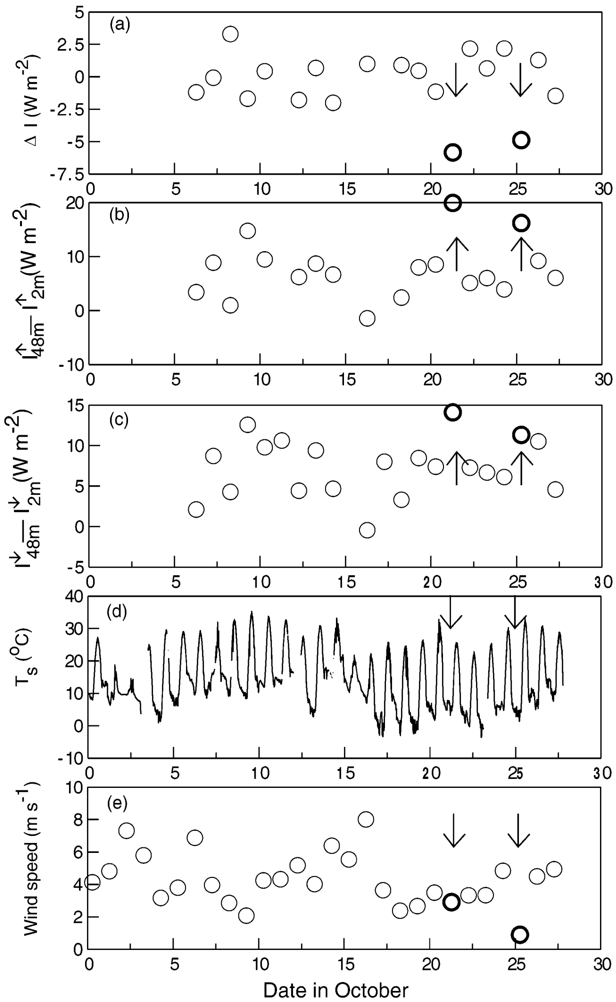

FIG. 13. Time series of (a) the net longwave radiative flux difference between 2 and 48 m, (b) the outgoing longwave radiation flux difference, (c) the incoming longwave radiation flux difference, (d) the surface radiation temperature at station 1, and (e) the 10-m wind speed at station 1. Each circle represents the average between 1700 and 1800 CST. The abscissa is the date in Oct 1999. The nights of 21 and 25 Oct are marked with the arrows in all the panels.

perature ensures a warm boundary layer and large downward longwave radiation in the early evening. The warm ground and weak wind ensure a large longwave emission from the ground in the early evening, which decreases sharply as the ground cools. The large downward longwave radiation and the sharp reduction of the upward longwave radiation both lead to large radiative flux divergence in the early evening. Although the maximum daytime surface radiation temperature on 26 October was highest following a 4-day warming trend, the wind speed of 4 m s^{-1} in the early evening increased vertical mixing and reduced the vertical temperature gradient in the observed layer, leading to smaller radiative flux divergence when compared with that on 25 October. Detailed analysis on 25 October is not presented in this paper because of its similarity to 21 October. The importance of the radiative flux divergence under weak-wind conditions was also shown by Gopalakrishnan et al. (1998).

Using the entire field campaign dataset, we found that the vertical difference of the outgoing radiative flux is positively related to the vertical temperature gradient and negatively related to the wind speed because strong wind leads to strong mixing (Fig. 14). Therefore, the vertical difference of the outgoing longwave radiative flux increases with the bulk Richardson number (Fig. 15).

The radiative flux divergence, on average, is smaller than the sensible heat flux divergence between 2 and 48 m at night (Fig. 12). However, the standard deviation of both the local cooling and the cooling due to the sensible heat flux divergence at a given hour is much larger than the cooling due to the radiative flux divergence. This result means that the radiative cooling is relatively consistent every night whereas the local cooling and the cooling due to the sensible heat flux divergence vary significantly from night to night.

Averaged over all of the nights from the field campaign, the vertical variation of the sensible heat flux is more than 10% below 20-m height (Fig. 16). In addition, on timescales of several hours, the departure of the sensible heat flux from the averaged value at each level varies with height, and the difference is often more than 10% of the averaged sensible heat flux. The M–O similarity theory assumes less than 10% vertical variation of the sensible heat flux and negligible radiative flux divergence within the surface layer. Based on this and previous studies, these requirements can be violated on any specific night, especially under very stable conditions and close to the ground where both the radiative and sensible heat flux divergences are relatively large.

5. Concluding remarks

Radiative flux divergence (2 levels) and sensible heat flux divergence (8 levels) were both directly measured in the nocturnal stable boundary layer during CASES-99. The radiative flux divergence was measured for the first time over a relatively deep layer (between 2 and 48 m) in contrast to earlier measurements within 10 m above the ground. Based on four downward-looking pyrgeometers at 2 m over four major surface types that were viewed by the downward-looking pyrgeometers at 48 m, the longwave emission at 2 m was calculated as if it were measured by a pyrgeometer with the same field of view as the one at 48 m.

The radiative flux observation indicates that the strongest radiative flux divergence occurs at the beginning of night when the ground cools rapidly and wind is weak. Under weak-wind and clear-sky conditions in the early evening, following a day with high surface radiation temperature and warm boundary layer, the ground cools very quickly while the rest of the boundary layer stays warm. The rapid decrease of the ground temper-

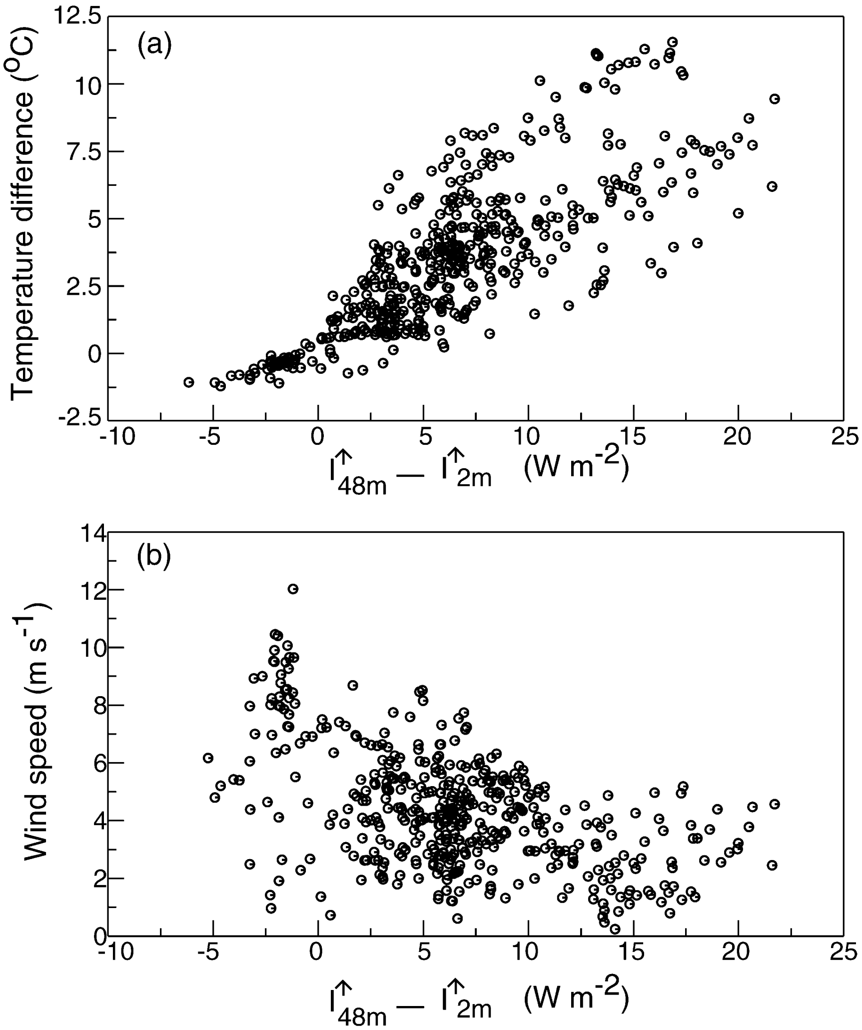

FIG. 14. Relationship between the outgoing longwave radiative flux difference between 2 and 48 m and (a) the temperature difference between 2.3 and 47.1 m and (b) wind speed at 15 m on the 60-m tower.

ature and, thus, the sharp decrease in the longwave radiation emission dominate the change in the radiative flux divergence as the incoming radiative flux decreases steadily over night. The radiative flux divergence in the early evening is controlled by how warm the surface becomes during the day and how fast the ground cools. The rapidly cooled ground and residual daytime turbulence lead to downward/zero sensible heat flux close to the ground and upward/zero sensible heat flux higher up, resulting in sensible heat flux divergence. Therefore, the radiative flux divergence and the sensible heat flux divergence both contribute to the rapid cooling of the air layer between 2 and 48 m at the beginning of the night.

The observed smaller longwave radiative cooling in comparison with the local cooling over the deep layer is different from the early radiation measurements in which the longwave radiative cooling was generally larger than the local cooling in a shallow layer close to the ground. The differences may be due to the vertical variation of the radiative flux divergence as suggested by radiation models. The vertical variation of the longwave radiative cooling and the local cooling implies that the relative contributions of the sensible heat divergence and the temperature advection (both horizontal and vertical) to the local cooling may also vary with height. The close relationship between the time variation of the local cooling and the radiative cooling between 2 and 48 m suggests that the radiative cooling is the primary heat sink at night.

This unique observation of the vertical variation of both radiative and sensible heat fluxes demonstrates the importance of the temperature advection (both horizontal and vertical) in the local cooling at night over a gently rolling surface. This result implies that previous studies of the nocturnal heat balance based only on ver-

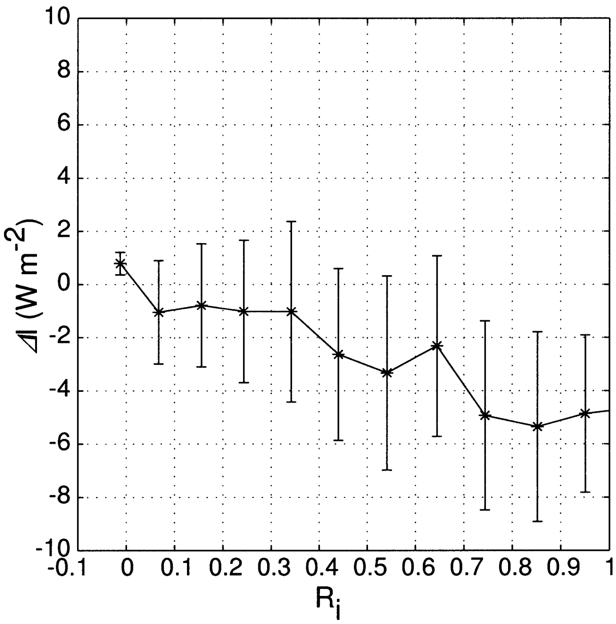

FIG. 15. Bin-averaged net radiative flux difference and the bulk Richardson number based on the 5-min-averaged dataset, with the standard deviation of the data within each bin. The Richardson number is calculated using the wind and temperature at 5 and 15 m on the 60-m tower. Data are from 1800 to 0600 CST.

tical variations of the radiative flux and assuming no advection may lead to wrong conclusions about the role of sensible heat flux in the local cooling.

The outgoing longwave radiation from the ground tends to fluctuate with wind speed because of variations in the area exposure of the warmer grass stems and soil surface and relatively cool tips of grass blades to the cold sky. The fluctuation of the outgoing longwave radiation from the ground leads to the fluctuation of the radiative flux divergence, which cannot be simulated by all of the radiation models. In general, the vertical difference of the outgoing longwave radiative flux between 2 and 48 m increases with the vertical temperature gradient and decreases with wind speed because of the vertical mixing and reduction of the vertical temperature gradient. The local 2-m air temperature tends to follow topography when wind speed is less than 5 m s^{-1} and is more uniform when wind speed is stronger than 5 m s^{-1}. The height-dependent temperature distribution may be due to local shallow drainage flows.

Our study indicates that the radiative flux divergence between 2 and 48 m is close to zero except in the early evening. However, it can be significant close to the ground based on the radiative flux divergence below 10 m in the earlier studies. On average, the radiative flux divergence increases with stability. The vertical variation of the sensible heat flux is found to be more than

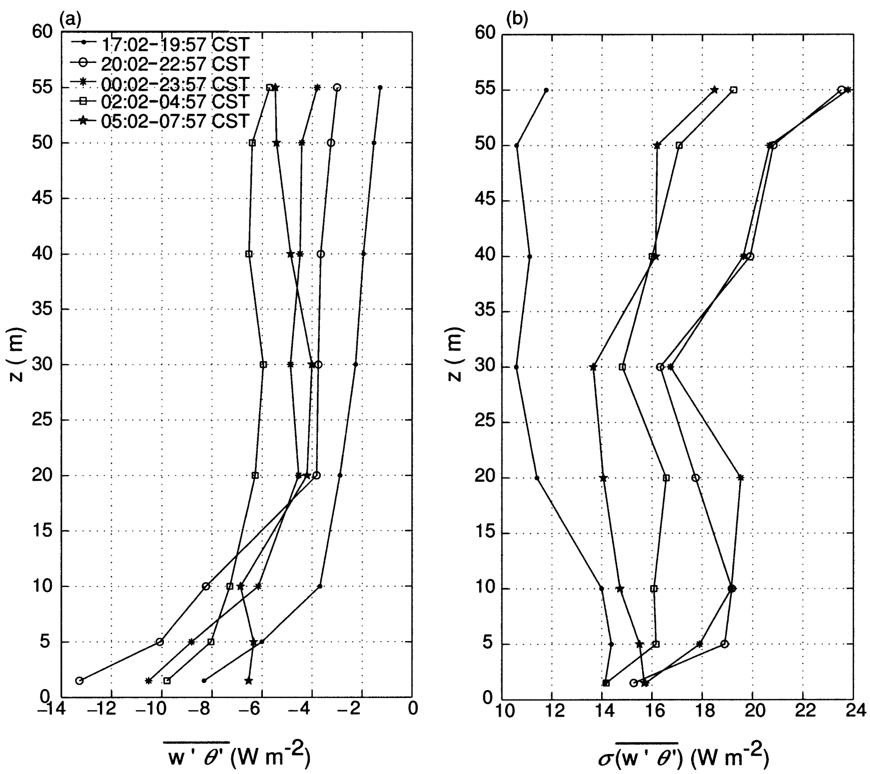

FIG. 16. (a) Vertical profiles of the sensible heat flux at various hours averaged over the entire field campaign. (b) The standard deviation of the sensible heat flux used to take the composite of the vertical profiles in (a) at the corresponding time period.

10% of its mean below 20 m. Therefore, the conditions for application of M–O similarity theory are often violated in the surface layer in the early evening and below 10 m above the ground at night because of the large radiative and sensible heat flux divergences.

Acknowledgments. The work was supported by Army Research Office DAAD19-99-1-0320 and National Science Foundation ATM-9906637. The 60-m tower and the six ISFF 10-m towers and the instruments on those towers were deployed by the National Center for Atmospheric Research (NCAR) Atmospheric Technology Division (ATD). We thank Larry Mahrt for his valuable comments. We also thank Argonne National Laboratory staff for their help during CASES-99. Thanks also go to *Journal of Applied Meteorology* editor Marvin Wesely, who will be sorely missed by the community.

APPENDIX A

Radiation Contribution from the 60-m Tower

If one assumes the tower is a solid rectangular block with width w in the north–south direction, and height H (Fig. A1), the upward longwave radiation measured by the pyrgeometer mounted on the 5-m boom at 48-m height can be approximated as

$$I^{\uparrow}_{48\mathrm{m}} = \frac{1}{2\pi}\left[\int_{-\alpha}^{\alpha}\int_{0}^{\beta_1} I_t \sin(2\theta)\, d\theta\, d\psi + \left(\int_{0}^{2\pi}\int_{\beta_1}^{\pi/2} + \int_{2\alpha}^{2\pi}\int_{0}^{\beta_2}\right) I_g \sin(2\theta)\, d\theta\, d\psi\right]$$
$$= \frac{1}{4\pi}\langle 2I_t\alpha[1 - \cos(2\beta_1)] + I_g\{2\pi[1 + \cos(2\beta_1)] + 4(\pi - \alpha)\}\rangle, \quad \text{(A1)}$$

using the angles defined in Fig. A1. Here, I_t and I_g represent the contribution from the tower and the ground surface, respectively. To focus on the contribution of the ground and the tower to the radiation measurement at 48 m, the layer of the atmosphere between the ground surface and the 48-m level is assumed to be transparent. Using the measurements listed in Table 2, (A1) becomes

$$I^{\uparrow}_{48\mathrm{m}} = 0.04I_t + 0.96I_g. \quad \text{(A2)}$$

Equation (A2) indicates that the influence of the tower is small because the tower structure occupies only a small portion of the field of view for the upward longwave radiation measured by the downward-looking pyrgeometer at 48 m, even though the tower structure is assumed to be a solid column.

In following the same analysis, the downward longwave radiation measured by the upward-looking pyrgeometer at 48 m can be approximated as

$$I^{\downarrow}_{48\mathrm{m}} = 0.03I_t + 0.97I_g. \quad \text{(A3)}$$

Equation (A3) indicates that the influence of the tower structure on the downward longwave radiation measured by the pyrgeometer at the 48-m level is also small.

APPENDIX B

Air-Layer Radiation Contribution between the Ground and 2 m

The contribution of the longwave radiation from the ground surface to a pyrgeometer I_g and from the uniform air layer below the measurement level of 2 m I_a to the longwave radiation measurement at z can be expressed as

$$I^{\uparrow}_{2\mathrm{m}} = I_g e^{-\tau} + \epsilon_a I_a, \quad \text{(B1)}$$

where τ is the optical thickness of the air layer and $\epsilon_a = 1 - e^{-\tau}$ is the emissivity of the air layer. The longwave radiation from the ground and from the air layer can be reduced further to

$$I_g = \epsilon_g \sigma T_g^4 \quad \text{and} \quad \text{(B2)}$$

$$I_a = \sigma T_a^4, \quad \text{(B3)}$$

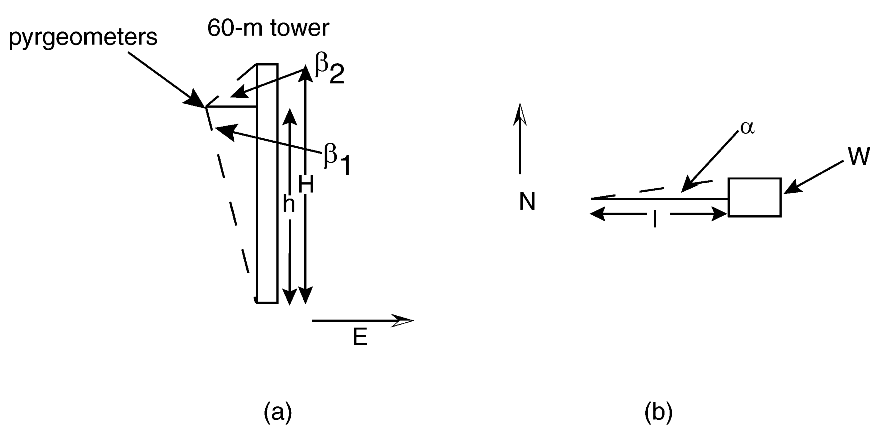

FIG. A1. Schematic diagram of the tower dimensions and angles relative to the pyrgeometers on the tower from looking (a) north and (b) downward.

where ϵ_g is the emissivity of the ground and T_a is the temperature of the air layer in kelvins. Because the ground is close to being a blackbody, the emissivity of the ground is assumed to be 1.

The emissivity ϵ_a can be calculated using the empirical formula in the appendix of André and Mahrt (1982). For simplification, we assume that the 2-m-deep homogeneous layer has a specific humidity of 10 g kg^{-1}, a temperature of 12°C, and a carbon dioxide concentration of 330 ppmv. This gives an emissivity of the air layer of about 0.2. This result implies that, at the measurement height of 2 m, the upward longwave radiation consists of 80% from the ground and 20% from the air. Equation (B1) can be expressed as

$$I_{2m}^{\uparrow} = 0.8\sigma T_g^4 + 0.2\sigma T_a^4. \tag{B4}$$

Because the Everest infrared surface temperature radiometer is a narrowband radiometer within the atmospheric window spectral band (8–14 μm), the influence of the atmosphere on the radiation measurement should be considerably smaller for an Everest IR radiometer than for a pyrgeometer at 2 m.

REFERENCES

Acevedo, O. C., and D. R. Fitzjarrald, 2001: The early evening surface layer transition: Temporal and spatial variability. *J. Atmos. Sci.,* **58,** 2650–2667.

André, J.-C., and L. Mahrt, 1982: The nocturnal surface inversion and influence of clear-air radiative cooling. *J. Atmos. Sci.,* **39,** 864–878.

Burns, S., and J. Sun, 2000: Thermocouple temperature measurements from the CASES-99 main tower. Preprints, *14th Symp. on Boundary Layer and Turbulence,* Snowmass, CO, Amer. Meteor. Soc., 358–361.

——, ——, A. C. Delany, T. W. Horst, and S. P. Oncley, 2000: Radiative flux divergence during CASES-99. Preprints, *14th Symp. on Boundary Layer and Turbulence,* Snowmass, CO, Amer. Meteor. Soc., 351–354.

——, ——, ——, S. R. Semmer, S. P. Oncley, and T. W. Horst, 2003: A field intercomparison technique to improve the relative accuracy of longwave radiation measurements and an evaluation of CASES-99 pyrgeometer data quality. *J. Atmos. Oceanic Technol.,* **20,** 348–361.

Campbell, G. S., and J. M. Norman, 1998: *An Introduction to Environmental Biophysics.* Springer, 286 pp.

Derbyshire, H., 1990: Nieuwstadt's stable boundary layer—Revisited. *Quart. J. Roy. Meteor. Soc.,* **116,** 127–158.

Elliott, W. P., 1964: The height variation of vertical heat flux near the ground. *Quart. J. Roy. Meteor. Soc.,* **90,** 260–265.

Fitzjarrald, D. R., and G. G. Lala, 1989: Hudson valley fog environments. *J. Appl. Meteor.,* **28,** 1303–1328.

Fuggle, R. F., and T. R. Oke, 1976: Long-wave radiative flux divergence and nocturnal cooling of the urban atmosphere. I: Above roof-level. *Bound.-Layer Meteor.,* **10,** 113–120.

Funk, J. P., 1960: Measured radiative flux divergence near the ground at night. *Quart. J. Roy. Meteor. Soc.,* **86,** 382–389.

Garratt, J. R., and R. A. Brost, 1981: Radiative cooling effects within and above the nocturnal boundary layer. *J. Atmos. Sci.,* **38,** 2730–2746.

Geiger, R., R. H. Aron, and P. Todhunter, 1995: *The Climate Near the Ground.* 5th ed. Vieweg, 528 pp.

Glaisher, J., 1847: On the amount of the radiation of heat, at night, from the earth, and from various bodies placed on or near the surface of the earth. *Philos. Trans. Roy. Soc. London,* **137,** 119–214.

Gopalakerishnan, S. G., M. Sharan, R. T. McNider, and M. P. Singh, 1998: Study of radiative and turbulent processes in the stable boundary layer under weak wind conditions. *J. Atmos. Sci.,* **55,** 954–960.

Grant, A. L. M., 1997: An observational study of the evening transition boundary-layer. *Quart. J. Roy. Meteor. Soc.,* **123,** 657–677.

Gustavsson, T., M. Karlsson, J. Bogren, and S. Lindqvist, 1998: Development of temperature patterns during clear nights. *J. Appl. Meteor.,* **37,** 559–571.

Harrison, A. A., 1971: A discussion of the temperatures of inland Kent with particular reference to night minima in the lowlands. *Meteor. Mag.,* **100,** 97–111.

Howell, J. F., and L. Mahrt, 1997: Multiresolution flux decomposition. *Bound.-Layer Meteor.,* **83,** 117–137.

——, and J. Sun, 1999: Surface layer fluxes in stable conditions. *Bound.-Layer Meteor.,* **90,** 495–520.

Kaimal, J. C., and J. J. Finnigan, 1994: *Atmospheric Boundary Layer Flows: Their Structure and Measurements.* Oxford University Press 289 pp.

Kobayashi, T., M. Mori, and K. Wakimizu, 1994: An observational study of a thermal belt on hillsides. *J. Meteor. Soc. Japan,* **72,** 387–399.

Kondo, J., O. Kanechika, and N. Yasuda, 1978: Heat and momentum transfers under strong stability in the atmospheric surface layer. *J. Atmos. Sci.,* **35,** 1012–1021.

LeMone, M. A., and R. M. Grossman, 2000: Mesoscale and diurnal variability of 2-m temperature. Preprints, *14th Symp. on Boundary Layer and Turbulence,* Snowmass, CO, Amer. Meteor. Soc., 5–8.

Lenschow, D. H., X.-S. Li, C.-J. Zhu, and B. B. Stankov, 1987: The stably stratified boundary layer over the Great Plains. Part I: Mean and turbulence structure. *Bound.-Layer Meteor.,* **42,** 95–121.

Li, Xing-sheng, J. E. Gaynor, and J. C. Kaimal, 1983: Study of multiple stable boundary layers in the nocturnal lower atmosphere. Studies of nocturnal stable layers at BAO, J. C. Kaimal, Ed., NOAA/ERL Wave Propagation Laboratory BAO Rep. 4, 129 pp. [NTIS PB83-209981]

Liou, K.-N., 1980: *Introduction to Atmospheric Radiation.* Academic Press, 392 pp.

Mahrt, L., J. Sun, W. Blumen, T. Delany, and S. Oncley, 1998: Nocturnal boundary-layer regimes. *Bound.-Layer Meteor.,* **88,** 255–278.

Maki, M., T. Harimaya, and K. Kikuchi, 1986: Heat budget studies on nocturnal cooling in a basin. *J. Meteor. Soc. Japan,* **64,** 727–740.

Moncrieff, J. B., 1983: The heat balance of the surface boundary layer at night. Ph.D. dissertation, University of Nottingham, 182 pp. [Available from the University of Nottingham, Department of Physiology and Environmental Science, School of Agriculture, Sutton Bonington, Loughborough, Leicestershire, United Kingdom.]

Monin, A. S., and A. M. Obukhov, 1954: Basic laws of turbulent mixing in the atmosphere near the ground. *Tr. Akad. Nauk SSSR Geofiz. Inst.,* **24,** 163–187.

Nieuwstadt, F. T. M., 1980: A rate equation for the inversion height in a nocturnal boundary layer. *J. Appl. Meteor.,* **19,** 1455–1447.

Nkemdirim, L. C., 1978: A comparison of radiative and actual nocturnal cooling rates over grass and snow. *J. Appl. Meteor.,* **17,** 1643–1646.

——, 1988: Nighttime surface-layer temperature tendencies with and without chinooks. *J. Appl. Meteor.,* **27,** 482–489.

Nunez, M., and T. R. Oke, 1976: Long-wave radiative flux divergence and nocturnal cooling of the urban atmosphere. II: Within an urban canyon. *Bound.-Layer Meteor.,* **10,** 121–135.

Ohya, Y. D., E. Neff, and R. N. Meroney, 1997: Turbulence structure in a stratified boundary layer under stable conditions. *Bound.-Layer Meteor.,* **83,** 139–161.

Oke, T. R., 1970: The temperature profile near the ground on calm clear nights. *Quart. J. Roy. Meteor. Soc.,* **96,** 14–23.

Poulos, G. S., and Coauthors, 2002: CASES-99: A comprehensive investigation of the stable nocturnal boundary layer. *Bull. Amer. Meteor. Soc.,* **83,** 555–581.

Qualls, R. J., and D. N. Yates, 2001: Directional radiometric temperature profiles within a grass canopy. *Adv. Water Res.,* **24,** 145–155.

Räisänen, P., 1996: The effect of vertical resolution on clear-sky radiation calculations: Tests with two schemes. *Tellus,* **48A,** 403–423.

Rider, N. E., and G. D. Robinson, 1951: A study of the transfer heat and water vapor above a surface of short grass. *Quart. J. Roy. Meteor. Soc.,* **77,** 375–401.

Roach, W. T., R. Brown, S. J. Caughey, J. A. Garland, and C. J. Readings, 1976: The physics of radiation fog: I—A field study. *Quart. J. Roy. Meteor. Soc.,* **102,** 313–333.

Smith, E. A., and L. Shi, 1992: Surface forcing of the infrared cooling profile over the Tibetan plateau. Part I: Influence of relative longwave radiative heating at high altitude. *J. Atmos. Sci.,* **49,** 805–822.

Stull, R. B., 1988: *An Introduction to Boundary Layer Meteorology.* Kluwer Academic, 666 pp.

Sun, J., 1999: Diurnal variations of thermal roughness height over a grassland. *Bound.-Layer Meteor.,* **92,** 407–427.

——, and Coauthors, 2002: Intermittent turbulence associated with a density current passage in the stable boundary layer. *Bound.-Layer Meteor.,* **105,** 199–219.

——, and Coauthors, 2004: Atmospheric disturbances that generate intermittent turbulence in nocturnal boundary layers. *Bound.-Layer Meteor.,* **110,** 255–279.

Tjemkes, S. A., and F. T. M. Nieuwstadt, 1990: A longwave radiation model for the nocturnal boundary layer. *J. Geophys. Res.,* **95,** 867–872.

Van Ulden, A. P., and J. Wieringa, 1996: Atmospheric boundary-layer research at Cabauw. *Bound.-Layer Meteor.,* **78,** 34–69.

Vining, R. C., and B. L. Blad, 1992: Estimation of sensible heat flux from remotely sensed canopy temperatures. *J. Geophys. Res.,* **97,** 18 951–18 954.

Yamada, T., 1979: Prediction of the nocturnal surface inversion height. *J. Appl. Meteor.,* **18,** 526–531.

Zhou, M., and Y. Chang, 1982: The wave properties in process of the nocturnal radiation inversion. *Mon. J. Sci.,* **3,** 156–159.

Zilitinkevich, S. S., and D. Mironov, 1996: A multi-limit formulation for the equilibrium depth of a stably stratified boundary layer. *Bound.-Layer Meteor.,* **81,** 325–351.